Lattice-Gas Models of Adsorption in the Double Layer<sup>1</sup>

Per Arne Rikvold <sup>a,b, 2, 3</sup>, Jun Zhang <sup>a</sup>, Yung-Eun Sung <sup>c</sup> and Andrzej Wieckowski <sup>c</sup>

#### Abstract

The theory of statistical-mechanical lattice-gas modeling of adsorption is reviewed and shown to be applicable to a range of electrochemical problems dominated by effective, lateral adsorbate-adsorbate interactions. A general strategy for applying the method to specific systems is outlined, which includes microscopic model formulation, calculation of zero-temperature phase diagrams, numerical calculation of thermodynamical and structural quantities at nonzero temperatures, and estimation of effective, lateral interaction energies that cannot be obtained by first-principles methods. Phenomena that are discussed include poisoning and enhanced adsorption, and illustrative applications to specific systems are reviewed. Particular problems considered are: the poisoning by sulfur of hydrogen adsorption on platinum (111), the electrochemical adsorption of naphthalene on polycrystalline copper and of urea on single-crystal platinum (100), and the underpotential deposition of copper on single-crystal gold (111).

Keywords: solid-liquid interfaces, coadsorption, phase transitions, theoretical modeling, numerical simulation.

<sup>&</sup>lt;sup>a</sup> Supercomputer Computations Research Institute, Florida State University, Tallahassee, Florida 32306-4052, USA

<sup>&</sup>lt;sup>b</sup> Center for Materials Research and Technology, and Department of Physics, Florida State University, Tallahassee, Florida 32306-3016, USA

<sup>&</sup>lt;sup>c</sup> Department of Chemistry and Frederick Seitz Materials Research Laboratory, University of Illinois, Urbana, Illinois 61801, USA

<sup>&</sup>lt;sup>1</sup>Submitted to *Electrochimica Acta*.

<sup>&</sup>lt;sup>2</sup>Electronic address: rikvold@scri.fsu.edu.

<sup>&</sup>lt;sup>3</sup>Corresponding author.

### 1 Introduction

Statistical-mechanical lattice-gas modeling provides a paradigm for analyzing site-specific single- and multicomponent chemisorption at electrode—electrolyte interfaces. The method is particularly useful to describe spatial ordering and fluctuations in the contact-adsorbed layer, which are strongly influenced by effective, lateral adsorbate—adsorbate interactions. The history of successful lattice-gas studies of phase transitions at solid—vacuum and solid—gas interfaces [1] makes the early applications of the method to double-layer studies [2, 3, 4, 5, 6, 7, 8, 9, 10, 11, 12, 13] excellent examples of the transfer of a methodology from one research area to another.

Here we present a condensed review of the basics of lattice-gas modeling of specific adsorption in the double-layer region, including a short discussion of poisoning and enhancement effects and illustrated by results from recent studies of specific systems. The outline of the remainder of the paper is as follows. In Sec. 2 we briefly review the lattice-gas formulation and some of the methods that can be used to obtain specific numerical results for such experimentally measurable quantities as adsorption isotherms, voltammetric currents and charge densities, and images obtained by low-energy electron diffraction (LEED) and atomic-resolution microscopies, such as scanning tunneling microscopy (STM) and atomic force microscopy (AFM). In particular we concentrate on non-perturbative numerical methods, such as Monte Carlo (MC) simulations [4, 14, 15, 16, 17, 18, 19, 20, 21, 22, 23] and transfer-matrix (TM) calculations [2, 3, 4, 11, 24, 25, 26, 27], which are often combined with finite-size scaling methods [22, 27, 28]. In Sec. 3 we briefly consider, within the lattice-gas picture, such nonlinear effects in multicomponent adsorption as poisoning [2, 3, 4, 10, 12, 13, 29] and enhanced adsorption [3, 10, 11, 12, 13, 29, 30], both with semiquantitative applications to specific systems. Reference [12] contains more extensive discussions and comparisons of these phenomena, which are just as relevant at solidvacuum and solid-gas interfaces as they are in electrochemistry, and which also can be extended to multilayer adsorption [30]. In Sec. 4 we provide further quantitative illustrations in the form of applications to two specific cases of adsorption on single-crystal electrodes: the electrosorption of urea on Pt(100) from an acid electrolyte [13, 14, 15, 16, 17, 18, 31] and the underpotential deposition (UPD) of copper on Au(111) from a sulfate-containing electrolyte [6, 7, 8, 9, 19, 20, 32, 33, 34, 35]. A final summary and conclusions

## 2 The Lattice-Gas Method

The lattice-gas models discussed here are defined through a generalization of the standard three-state lattice-gas Hamiltonian (energy function) used, e.g., in Refs. [2, 3, 4, 11, 12, 13], to give the energies of particular adsorbate configurations:

$$\mathcal{H}_{LG} = \sum_{n} \left[ -\Phi_{AA}^{(n)} \sum_{\langle ij \rangle}^{(n)} c_{i}^{A} c_{j}^{A} - \Phi_{AB}^{(n)} \sum_{\langle ij \rangle}^{(n)} \left( c_{i}^{A} c_{j}^{B} + c_{i}^{B} c_{j}^{A} \right) - \Phi_{BB}^{(n)} \sum_{\langle ij \rangle}^{(n)} c_{i}^{B} c_{j}^{B} \right] + \mathcal{H}_{3} - \bar{\mu}_{A} \sum_{i} c_{i}^{A} - \bar{\mu}_{B} \sum_{i} c_{i}^{B} .$$
(1)

Here  $c_i^{\rm X} \in \{0,1\}$  is the local occupation variable for species X (X=A or B), and the third adsorption state ("empty" or "solvated") corresponds to  $c_i^{\rm A} = c_i^{\rm B} = 0$ . The sums  $\sum_{\langle ij \rangle}^{(n)}$  and  $\sum_i$  run over all nth-neighbor bonds and over all adsorption sites, respectively,  $\Phi_{\rm XY}^{(n)}$  denotes the effective XY pair interaction through an nth-neighbor bond, and  $\sum_n$  runs over the interaction ranges. The term  $\mathcal{H}_3$  contains three-particle [36] and possibly multi-particle interactions. Both the interaction ranges and the absence or presence of multi-particle interactions depend on the specific system. The change in electrochemical potential when one X particle is removed from the bulk solution and adsorbed on the surface is  $-\bar{\mu}_{\rm X}$ . The sign convention is such that  $\Phi_{\rm XY}^{(n)} > 0$  denotes an effective attraction, and  $\bar{\mu}_{\rm X} > 0$  denotes a tendency for adsorption in the absence of lateral interactions.

The main differences between models for particular systems are the bindingsite geometries of the adsorbed species and the strengths of the effective, lateral interactions. (Straightforward modifications of Eq. (1) are necessary if the adsorption sites for the two species are different, as they are, e.g., in the model describing urea on Pt(100).) Some previously studied models that can be defined by Eq. (1) or similar lattice-gas Hamiltonians, are the one for urea on Pt(100) [13, 14, 15, 16, 17, 18, 31], the model developed by Huckaby and Blum for UPD of copper on Au(111) in the presence of sulfate [6, 7, 8, 9, 19, 20, 32, 33, 34, 35], and the standard three-state models with single-site bonding, used in previous studies of poisoning and enhancement in multicomponent adsorption [3, 4, 11, 12, 13]. As illustrations of the lattices and interactions that can be used, we show in Fig. 1 the model used for urea adsorption on Pt(100) [13, 14, 15, 16, 17, 18, 31] and in Fig. 2 one used for copper UPD on Au(111) [19, 20].

The thermodynamic density conjugate to the electrochemical potential  $\bar{\mu}_X$  in Eq. (1) is the surface coverage by species X,

$$\Theta_{\mathcal{X}} = N^{-1} \sum_{i} c_i^{\mathcal{X}} , \qquad (2)$$

where N is the total number of surface unit cells in the system. To connect the electrochemical potentials to the bulk concentrations [X] and the electrode potential E, one has (in the weak-solution approximation):

$$\bar{\mu}_{\rm X} = \mu_{\rm X}^0 + RT \ln \frac{[{\rm X}]}{[{\rm X}]^0} - z_{\rm X} FE ,$$
 (3)

where R is the molar gas constant, T is the absolute temperature, F is Faraday's constant, and the effective electrovalence of X is  $z_X$ . The quantities superscripted with a 0 are reference values which contain the local binding energies to the surface. They are generally temperature dependent due, among other effects, to rotational and vibrational modes.

In the absence of diffusion and double-layer effects and in the limit that the potential sweep rate  $dE/dt\rightarrow 0$  [37], the voltammetric current i per unit cell of the surface is the time derivative of the charge transported across the interface during the adsorption/desorption process. With a sign convention such that oxidation/anodic currents are considered positive, this charge is

$$q = -e(z_{A}\Theta_{A} + z_{B}\Theta_{B}), \qquad (4)$$

where e is the elementary charge unit. Using partial differentiation involving the relation between the electrode potential and the electrochemical potentials, Eq. (3), as well as the Maxwell relation  $\partial \Theta_{\rm A}/\partial \bar{\mu}_{\rm B} = \partial \Theta_{\rm B}/\partial \bar{\mu}_{\rm A}$ , one obtains i in terms of the lattice-gas response functions  $\partial \Theta_{\rm X}/\partial \bar{\mu}_{\rm Y}$ :

$$i = e\mathcal{F} \left\{ z_{\rm A}^2 \frac{\partial \Theta_{\rm A}}{\partial \bar{\mu}_{\rm A}} + 2z_{\rm A} z_{\rm B} \frac{\partial \Theta_{\rm B}}{\partial \bar{\mu}_{\rm A}} + z_{\rm B}^2 \frac{\partial \Theta_{\rm B}}{\partial \bar{\mu}_{\rm B}} \right\} \frac{\mathrm{d}E}{\mathrm{d}t} . \tag{5}$$

It must be emphasized that the interactions in Eq. (1) are effective interactions mediated through several channels. The mechanisms involved include interactions between the adsorbate and the substrate electron structure [38, 39, 40, 41, 42], adsorbate-induced local deformations of the substrate, interactions with the fluid electrolyte [5, 6, 7, 8, 9, 11, 32, 33, 34, 35], and (screened) electrostatic interactions [43]. All these effects give rise to indirect, effective interactions between the adsorbate particles. In general one must assume that these quantities could be dependent on temperature and electrode potential. The spatial structure of the generalized pair interactions generally involves rather complicated dependences on both the magnitude and the direction of the vector joining the two adsorbate particles, as well as on the relative orientation of the particles. Empirical models for the electronic contribution to the effective, lateral pair interactions are well known [38, 39, 40, 41, 42] and are often of a decaying, oscillatory form proportional to  $\cos(2k_{\rm F}r)/r^{\alpha}$ , where  $k_{\rm F}$  is the Fermi momentum and  $\alpha$  may be between 2 and 5, depending on the substrate's electronic structure [39, 40]. However, changes in the effective interaction energies of only a few percent may cause very substantial changes in the finite-temperature phase diagram (see, e.g., Refs. [44, 45, 46]). First-principles calculations of lateral adsorbate interactions to this level of accuracy are not yet feasible, even for the electronically mediated contributions [42].

Here we advocate an approach to the problem of determining the effective adsorbate—adsorbate interaction energies, which provides a practical alternative to the ideal "first-principles" approach mentioned above. This strategy consists in fitting the thermodynamic and structural predictions of the lattice-gas model directly to experiments, taking into account as wide a spectrum of experimental information as possible. Obviously, this method also involves considerable difficulties. In particular, the number of parameters that can reasonably be included in a lattice-gas model is large, and there is no a priori guarantee that a minimal set of fitted interactions is unique. Nevertheless, the encouraging results of previous lattice-gas studies of electrochemical systems that have employed this strategy [2, 3, 4, 5, 6, 7, 8, 9, 10, 11, 12, 13, 14, 15, 16, 17, 18, 19, 20, 32, 33, 34, 35] indicate that when proper attention is paid to including all available experimental information in a consistent fashion, the predictive power of this approach is considerable. Furthermore, as effective interactions obtained by first-principles calculations become available in the future, the results obtained from latticegas models will provide crucial information for testing the consistency of such first-principles interactions with the experimentally observed thermodynamic and structural information. The steps in the modeling strategy outlined here can be summarized as follows.

- 1. Use prior theoretical and experimental knowledge about the adsorbate lattice structure and lattice constant and the shapes and sizes of the adsorbate particles to formulate a specific lattice-gas model. Examples are shown in Figs. 1 and 2.
- 2. Use available experimental information about adsorbate coverages and adlayer structure to determine the adsorbate phases or at least narrow down the possible choices as much as possible.
- 3. Perform a group-theoretical ground-state calculation [47, 48, 49] to determine a minimal set of effective interactions compatible with the observed adsorbate phases. Relations between the effective interactions take the form of a set of inequalities [2, 3, 4, 11, 12]. A ground-state diagram (zero-temperature phase diagram) is obtained by pairwise equating the ground-state energies of the different phases. Examples of ground-state diagrams corresponding to the specific models in Figs. 1 and 2 are shown in Figs. 3 and 4, respectively. 4. At nonzero temperatures, the thermodynamic and structural properties of the lattice-gas model constructed through steps 1–3 can be studied by a number of analytical and numerical methods, depending on the quantities of interest and the complexity of the Hamiltonian. These methods include mean-field approximations [10, 29] (although these can be unreliable for lowdimensional systems with short-range interactions [44]), Padé-approximant methods based on liquid theory [6, 7, 8, 9, 32, 33, 34, 35], numerical TM calculations [2, 3, 4, 11, 12, 13], and MC simulations [4, 14, 15, 16, 17, 18, 19, 20]. 5. Whatever method is used to calculate the finite-temperature properties of the model, these should be used to refine the effective interactions by comparison with the available experiments, or by obtaining additional experimental data for such comparison.

Steps 4 and 5 should be iterated until satisfactory agreement between model and experiment is achieved.

One of the main reasons for the rapid expansion in theoretical surface science over the last three decades is the development of numerical methods that allow nonperturbative calculations of thermal and structural properties of statistical-mechanical systems. Two such methods, which are particularly well suited to the study of lattice-gas models, are Monte Carlo (MC) simulation [4, 14, 15, 16, 17, 18, 19, 20, 21, 22, 23] and numerical transfermatrix (TM) calculations [2, 3, 4, 11, 24, 25, 26, 27]. In combination with finite-size scaling analysis of phase-transition phenomena [22, 27, 28], these

methods have contributed significantly to the theoretical understanding of fluctuations and ordering at surfaces and interfaces. The reason for our emphasis on non-perturbative numerical methods is that they are much more accurate for two-dimensional systems than even quite sophisticated mean-field approximations [44], yet they are quite easy to program. Moreover, with modern computer technology their implementation is well within the resources of most researchers.

At present, a large number of monographs and textbooks exist that describe MC methods in great detail [21, 22, 23]. We therefore limit ourselves to pointing out that these methods can produce thermodynamic and structural information for a variety of systems, with a very modest amount of programming and with computational resource needs that are readily met by modern workstations. For example, all the MC results presented here were obtained on workstations. For studies of real systems, MC models have the advantage that programs are relatively easy to modify to accommodate changes in lattice structure and/or interaction geometries and ranges.

Despite their power and beauty, TM methods are much less known outside the statistical-mechanics community. However, good reviews are available [24, 27], and simple textbook expositions for the one-dimensional case are quite illustrative [25, 26]. An abundance of details are scattered throughout the technical literature and can be found, together with further references in e.g. Refs. [2, 3, 4, 11, 50, 51]. Briefly, the method allows the numerical calculation of free energies (an advantage over MC, which does not easily produce entropies), thermodynamic densities, and their associated response functions from the eigenvalues and eigenvectors of a matrix of Boltzmann factors, called the transfer matrix. In addition to the ability to easily calculate free energies, the method has the further advantage over MC that the results are obtained without statistical errors. The main disadvantages, relative to MC, are the limited system sizes and interaction ranges that can be attained. The first problem can relatively easily be overcome with finite-size scaling. The second, however, severely restricts the applicability of TM methods to realistic electrochemical systems.

# 3 Poisoning and Enhancement Effects

Depending on the relative interaction ranges and strengths, the lattice-gas models discussed in Sec. 2 allow many topologically different adsorbate phase diagrams. The specific coadsorption phenomena, such as poisoning [2, 3, 4, 10, 12, 13, 29] or enhanced adsorption [3, 10, 11, 12, 13, 29, 30], which occur for any particular set of interactions, depend crucially on the detailed topology of the phase diagram [2, 3, 4, 11, 12, 13]. The terms "poisoning" and "enhancement" can be defined as follows.

Poisoning of A by B: When  $\bar{\mu}_B$  is increased at constant  $\bar{\mu}_A$ , the total coverage,  $\Theta_A + \Theta_B$ , goes through a minimum as  $\Theta_A$  decreases sharply with only a small corresponding increase in  $\Theta_B$ .

Enhancement of A by B:  $\Theta_A$  goes through a maximum as  $\bar{\mu}_B$  is increased at constant  $\bar{\mu}_A$ . For large  $\bar{\mu}_B$ , the enhancement gives way to substitutional desorption, each adsorbed B particle replacing one or more A particles.

For both poisoning and enhancement, a measure of the modification strength is the differential coadsorption ratio,  $d\Theta_A/d\Theta_B$ . The modification is characterized as strong if  $|d\Theta_A/d\Theta_B| > Z$ , the lattice coordination number. In Refs. [4, 11, 12] it was discussed in detail how the modification strength is related to the interaction constants for specific, triangular lattice-gas models through the shape of the adsorbate phase diagram. From the standpoint of statistical mechanics, strong modification results from fluctuations typical of the region near a line of critical end points, which joins a surface of discontinuous phase transitions to one of continuous transitions. More intuitively, these fluctuations can be described as follows. For poisoning, they correspond to an almost bare surface, from which the A particles are repelled by a very small coverage of repulsively interacting B particles [4]. In the case of enhanced adsorption, the corresponding picture is that of a surface almost fully covered by a monolayer of A particles, which is "pinned down" by a low concentration of attractively interacting B particles [11]. These considerations lead to inequalities that must be obeyed by the interaction constants, in order for the system to exhibit either poisoning or enhancement of various strengths. The inequalities are illustrated in Fig. 1 of Ref. [12] for triangular models with nearest-neighbor interactions.

### 3.1 An Example of Poisoning

An example of poisoning is provided by the model for the coadsorption of sulfur and hydrogen on Pt(111) in acid aqueous environment, studied by Rikvold and coworkers [2, 3, 4]. In this case, the effective nearest-neighbor lateral interactions were obtained from experimental thermodynamic and scattering data. The numerical adsorption isotherms (obtained by both MC and TM methods) gave maximum desorption ratios  $d\Theta_H/d\Theta_S \approx -7 \pm 1$ , in favorable agreement with experiments [52]. It was argued that the general shape of the phase diagram for this model is characteristic of strong poisoning behavior [4].

### 3.2 An Example of Enhancement

An application of lattice-gas models to study enhanced adsorption was given by Rikvold and Deakin [11], who analyzed experimental data for the electrosorption of organics on metal electrodes: naphthalene on copper [53] and n-decylamine on nickel [54]. They followed a suggestion by Damaskin et al. [55] that the potential dependence of adsorption of organics on metals can be attributed to the influence of coadsorbed hydrogen. Although the experimental results concerned rough, polycrystalline electrodes, a simple nearest-neighbor model on a triangular lattice was used, aiming merely for semiquantitative agreement. The effective electrovalences were taken as  $z_{\rm H}\!=\!+1$  and  $z_{\rm organic}\!=\!0$ , and the three effective interaction constants,  $\Phi_{\rm XY}$ , together with  $\mu_{\rm H}^0$  and  $\mu_{\rm organic}^0$ , were determined by nonlinear least-squares fits of numerical coadsorption isotherms obtained from a TM calculation to the experimental data. The experimental and fitted numerical adsorption isotherms for naphthalene on copper are shown in Fig. 5. The maxima are due to the formation of a mixed naphthalene/hydrogen adsorbed phase in the potential region between -1000 and -800 mV versus the normal hydrogen electrode (NHE). The fitted lattice-gas interactions are consistent with independent estimates [53, 54], as discussed in detail in Ref. [11].

# 4 Adsorption on Single-Crystal Surfaces

A major source of uncertainty in the applications of simple lattice-gas models to the experimental results discussed in the previous section, is the poor characterization of the electrode surfaces. To remedy this situation, Wieckowski and Rikvold with collaborators have undertaken a series of studies of the electrosorption of small molecules and ions on well-characterized single-crystal surfaces. A characteristic aspect of these systems is the high specificity of the adsorption phenomena with respect to the structures of the substrate lattice and the main adsorbate. A good geometric fit promotes the formation of ordered adsorbate phases commensurate with the substrate, which can be observed both by in situ atomic-scale spectroscopies and by ex situ scattering techniques. The detailed experimental results that can be extracted from such systems merit the construction of more complicated models with longer-ranged and multi-particle interactions.

By way of examples we discuss two specific single-crystal adsorption systems: the electrosorption of urea on Pt(100) from an acid electrolyte [13, 14, 15, 16, 17, 18, 31] and the UPD of copper on Au(111) from a sulfatecontaining electrolyte [6, 7, 8, 9, 19, 20, 32, 33, 34, 35]. Both systems exhibit a dramatic peak sharpening in the cyclic voltammogram (CV), from several hundred mV to on the order of 10 mV when a small concentration of the adsorbate species (urea, or a mixture of sulfate and copper ions, respectively) is added to the supporting electrolyte. This effect is also exhibited by other systems, such as sulfuric acid on Rh(111) [18, 31, 56]. Whereas the urea/Pt(100) system develops only a single, sharp CV peak [57], in the case of copper UPD, two peaks, approximately 100 mV apart, are exhibited [58, 59]. We associate these effects with phase transitions in the layer of contact adsorbed particles. These transitions involve the replacement of a monolayer of adsorbed hydrogen or copper on the negative-potential side of the CV peaks by ordered submonolayers at more positive potentials. The observed voltammetric changes are much weaker or absent when the same substances are adsorbed onto other crystal planes of the same metals [31, 57, 60]. The high specificity with respect to the adsorbent surface structure indicates that the effects depend crucially on the geometric fit between (at least one of) the adsorbate species and the surface. This observation was used in developing the specific lattice-gas models.

## 4.1 Urea on Pt(100)

In addition to the surface-specific narrowing of the CV peak upon the addition of urea to the supporting electrolyte, the experimental observations to

which the model was fitted are as follows. (For details, see Refs. [16, 18].)

- 1. The urea coverage  $\Theta_U$ , measured in situ by a radiochemical method (RCM), changes over a potential range of approximately 20 mV around the CV peak position from near zero on the negative side to approximately 1/4 monolayers (ML) on the positive side.
- 2. Ex situ Auger electron spectroscopy (AES) studies are consistent with the RCM results.
- 3. Ex situ LEED studies at potentials on the positive side of the CV peak show an ordered  $c(2\times4)$  adsorbate structure, consistent with an ideal coverage of 1/4 ML. Upon emersion on the negative side of the CV peak, only an unreconstructed  $(1\times1)$  surface is found.

The lattice-gas model developed to account for these observations was based on the assumption that urea  $[CO(NH_2)_2]$  coordinates the platinum through its nitrogen atoms (or NH<sub>2</sub> groups), with the C=O group pointing away from the surface. Since the unstrained N-N distance in urea matches the lattice constant of the square Pt(100) surface quite well (2.33 A [61] versus 2.77 Å [62]), it was assumed that urea occupies two adsorption sites on the square Pt(100) lattice. Integration of the CV profiles indicates that the hydrogen saturation coverage in the negative-potential region corresponds to one elementary charge per Pt(100) unit cell, and that most of the surface hydrogen is desorbed in the same potential range where urea becomes adsorbed. Therefore, it was assumed [13] that hydrogen adsorbs in the same on-top positions as the urea nitrogen atoms. This assumption was recently strengthened by visible-infrared sum generation spectroscopy observations [63, 64]. The resulting model [13] is a dimer-monomer model in which hydrogen is adsorbed at the nodes and urea on the bonds of a square lattice representing the Pt(100) surface. Simultaneous occupation of bonds that share a node by two or more urea molecules is excluded, as is occupation by hydrogen of a node adjacent to a bond occupied by urea. In order to stabilize the observed  $c(2\times4)$  phase, effective interactions were included through eighth-nearest neighbors [14, 15, 16, 17, 18, 31]. The configuration energies are given by Eq. (1) with A=U (urea) and B=H (hydrogen). The model is illustrated in Fig. 1 and its ground-state diagram in Fig. 3. The effective lattice-gas interactions were determined from ground-state calculations followed by numerical MC simulations.

The numerical simulations, which used systems with up to  $32\times32$  square-

lattice unit cells, were performed with a heat-bath MC algorithm [21, 22, 23] with updates of clusters consisting of five nearest-neighbor nodes arranged in a cross, plus their four connecting bonds. After symmetry reductions these clusters have 64 different configurations, and the corresponding code is rather slow in terms of machine time per MC step. However, the additional transitions allowed by these clusters, relative to minimal clusters consisting of two nodes and their connecting bond, include "diffusion-like" moves in which the urea molecules can go from one bond to another and the hydrogen atoms from one node to another, without changing the local coverages within the cluster. These moves significantly reduce the free-energy barriers that must be surmounted in order to locally minimize the adsorbate free energy, and they dramatically reduce the number of MC steps per site (MCSS) necessary for the system to reach thermodynamic equilibrium. For this system, simulated "LEED patterns" were obtained as the squared Fourier transform of the adsorbed urea configurations. These were obtained by the Fast Fourier Transform algorithm and averaged in the same way as the thermodynamic quantities [18].

Since the number of model parameters is large, the numerical calculations are time consuming, and the experimental data concern a number of different quantities, parameter estimation by a formal optimization procedure was not a practical alternative for this study. (This contrasts with the simpler situations discussed in Refs. [11, 44, 46], where a small number of lattice-gas parameters could be determined by a formal least-squares procedure to fit extensive experimental results for a single thermodynamic quantity.) To make maximum use of all available information, the model parameters were therefore varied "by hand", taking into consideration both the various experimental results and available chemical and physical background information, until acceptable agreement was obtained with room-temperature experimental results. In particular, agreement was sought between the shapes of the simulated and experimental CV profiles, as shown in Fig. 6. The resulting interactions are given in the caption of Fig. 1.

# 4.2 Copper UPD on Au(111)

Underpotential deposition (UPD) is a process whereby a monolayer or less of one metal is electrochemically adsorbed onto another in a range of electrode potentials more positive than those where bulk deposition would occur [37]. The UPD of copper on Au(111) electrodes in sulfate-containing electrolytes has been intensively studied, both experimentally (see discussion of the literature in Ref. [20]) and theoretically [6, 7, 8, 9, 19, 20, 32, 33, 34, 35]. The most striking feature observed in CV experiments with Au(111) electrodes in sulfate-containing electrolyte is the appearance of two peaks, separated by about  $100\sim150$  mV, upon the addition of Cu<sup>2+</sup> ions [58, 59]. Typical CV profiles are shown in Fig. 7, together with preliminary simulation results [19, 20]. In the potential range between the peaks, the adsorbate layer is believed to have a  $(\sqrt{3}\times\sqrt{3})$  structure consisting of 2/3 ML copper and 1/3 ML sulfate [6, 7, 8, 9, 20, 32, 33, 34, 35, 65, 66, 67].

The lattice-gas model for UPD of copper on Au(111) in sulfate-containing electrolyte, used in Refs. [19, 20], is a refinement of the model introduced and studied by Huckaby and Blum [6, 7, 8, 9, 32, 33, 34, 35]. It is based on the assumption that the sulfate coordinates the triangular Au(111) surface through three of its oxygen atoms, with the fourth S-O bond pointing away from the surface, as is also the most likely adsorption geometry on Rh(111) [18]. This adsorption geometry gives the sulfate a "footprint" in the shape of an approximately equilateral triangle with a O-O distance of 2.4 Å [68], reasonably matching the lattice constant for the triangular Au(111) unit cell, 2.88 Å [62]. The copper is assumed to compete for the same adsorption sites as the sulfate. The configuration energies are given by Eq. (1) with A=S (sulfate) and B=C (copper). The model is illustrated in Fig. 2 and its ground-state diagram in Fig. 4.

It has been experimentally observed [66, 67] that sulfate remains adsorbed on top of the copper monolayer in the negative-potential region. In principle, this system should therefore be described by a multilayer lattice-gas model [30]. In Refs. [19, 20] this complication was avoided by using the following, simple mean-field estimate for the sulfate coverage in this second layer:

$$\Theta_{\rm S}^{(2)} = \alpha \Theta_{\rm C} (1/3 - \Theta_{\rm S}) , \qquad (6)$$

which allows the difference between the first-layer coverage  $\Theta_{\rm S}$  and its saturation value of 1/3 to be transferred to the top of the copper layer. The factor  $\alpha$  is a phenomenological constant. Since the transfer of sulfate between the gold and copper surfaces does not involve an oxidation/reduction process, the total charge transport per unit cell during the adsorption/desorption process becomes

$$q = -e[z_{\rm s}(\Theta_{\rm S} + \Theta_{\rm S}^{(2)}) + z_{\rm C}\Theta_{\rm C}], \qquad (7)$$

giving a CV current density which reduces to that of Eq. (5) for  $\alpha=0$ :

$$i = eF \left\{ z_{\rm S}^2 (1 - \alpha \Theta_{\rm C}) \left. \frac{\partial \Theta_{\rm S}}{\partial \bar{\mu}_{\rm S}} \right|_{\bar{\mu}_{\rm C}} + z_{\rm C} (z_{\rm C} - 2\alpha z_{\rm S} \Theta_{\rm S}/3) \left. \frac{\partial \Theta_{\rm C}}{\partial \bar{\mu}_{\rm C}} \right|_{\bar{\mu}_{\rm S}} + z_{\rm S} (2z_{\rm C} + \alpha z_{\rm S} (1/3 - \Theta_{\rm S}) - \alpha z_{\rm C} \Theta_{\rm C}) \left. \frac{\partial \Theta_{\rm S}}{\partial \bar{\mu}_{\rm C}} \right|_{\bar{\mu}_{\rm S}} \right\} \frac{dE}{dt} . \tag{8}$$

The effective electrovalences,  $z_{\rm S}$  and  $z_{\rm C}$ , must be determined from experiments [65, 66, 67]. In Refs. [19, 20] the approximate values,  $z_{\rm C}$ =+2 and  $z_{\rm S}$ =-2, were used.

The ground-state diagram corresponding to the interactions used in Refs. [19, 20] is shown in Fig. 4. For large negative  $\bar{\mu}_{\rm S}$ , only copper adsorption is possible, and the phase diagram is that of the lattice-gas model corresponding to the triangular-lattice antiferromagnet with next-nearest neighbor ferromagnetic interactions [69]. Similarly, in the limit of large positive  $\bar{\mu}_{\rm S}$  and large negative  $\bar{\mu}_{\rm C}$ , the zero-temperature phase is the  $(\sqrt{3} \times \sqrt{3})_0^{1/3}$  sulfate phase characteristic of the hard-hexagon model [7, 8, 9, 32, 33, 34, 35, 70]. The phase diagram for intermediate electrochemical potentials is quite complicated.

To obtain adsorption isotherms and CV currents at room temperature, MC simulations were performed on a 30×30 triangular lattice, using a heat-bath algorithm [21, 22, 23] with updates at randomly chosen sites. In order to avoid getting stuck in metastable configurations (a problem which is exacerbated by the nearest-neighbor sulfate-sulfate exclusion), clusters consisting of two nearest-neighbor sites were updated simultaneously.

The potential scan path corresponding to the CV shown in Fig. 7 is indicated by the dotted line labeled "1" in the ground-state diagram, Fig. 4. With the aid of this diagram, it is easy to analyse the simulation results. As was pointed out above, there is experimental evidence that at the negative end of the UPD potential range, sulfate adsorbs in a neutral submonolayer on top of the monolayer of copper, with a coverage  $\Theta_S^{(2)} \approx 0.2$  [66, 67]. This corresponds to  $\alpha = 0.6$  in Eq. (6), which was used to obtain the simulated CV current shown in Fig. 7. Starting from the negative end, we scan in the direction of positive electrode potential (upper left to lower right in Fig. 4). Near the CV peak at approximately 70 mV, the sulfate begins to compete with copper for the gold surface sites, resulting in a third of the copper desorbing into the bulk and being replaced by sulfate. The potential range over

which the replacement takes place corresponds to a peak width of about 30 mV. Due to the strong effective attraction between the copper and sulfate adparticles, a mixed  $(\sqrt{3} \times \sqrt{3})_{2/3}^{1/3}$  phase is formed, which extends through the entire potential region between the two CV peaks. As the CV peak at approximately 170 mV is reached, most of the copper is desorbed within a potential range of about 20 mV. As it is thus deprived of the stabilizing influence of the coadsorbed copper, the sulfate is partly desorbed, reducing  $\Theta_{\rm S}$ from 1/3 to approximately 0.16. This system provides another illustrative example of the enhanced adsorption phenomenon described in Sec. 3.2. The  $(\sqrt{3}\times\sqrt{7})_0^{1/5}$  phase found in the potential region near 200 mV is consistent with experimental observations on copper free systems [71, 72]. Eventually, more positive electrode potentials cause the sulfate to form its saturated  $(\sqrt{3}\times\sqrt{3})_0^{1/3}$  hard-hexagon phase. However, in the model, this transition occurs at a somewhat more negative potential than is observed experimentally [65, 66, 67]. The scenario described here corresponds closely to that proposed by Huckaby and Blum [6, 7, 8, 9, 32, 33, 34, 35]. The agreement between the experimental and theoretical results is reasonable, except for large positive E, where the model predicts less copper and more sulfate on the surface than indicated by the experiments. The heights of the CV peaks predicted by the model are larger than what is observed in experiments, a discrepancy which is probably due to defects on the electrodes used in the experiments.

## 5 Conclusion

We have briefly reviewed the application of statistical-mechanical lattice-gas modeling to specific adsorption in the double-layer region. The method is well suited to describe ordering and fluctuation effects in the contact-adsorbed layer, which are strongly influenced by effective, lateral interactions. Phenomena that can be described include poisoning and enhancement effects, and concrete examples were given for several systems of experimental interest. The effective interactions arise from a number of different sources, including mediation through the substrate electrons, through phonons, and through the fluid near the surface, and their calculation from first principles is not yet feasible in general. The alternative route advocated here provides a microscopic picture of the adsorbate structure, as well as a procedure for estimating approximate effective interaction energies from experimentally ob-

served structural and thermodynamic quantities. The resulting models have considerable predictive power regarding the dependences of observed thermodynamic quantities on the electrochemical potential and the bulk solute concentrations, as well as on the geometric structure of the substrate and the adsorbates. Since the methods discussed are simple to program and not particularly computationally intensive, they are well suited for experimental data analysis.

#### Acknowledgement

We acknowledge useful discussions with L. Blum. Helpful comments on the manuscript were provided by M. A. Novotny, R. A. Ramos, H. L. Richards, and S. W. Sides. This research was supported by the Florida State University (FSU) Supercomputer Computations Research Institute under US Department of Energy Contract No. DE-FC05-85ER25000, by the FSU Center for Materials Science and Technology, and by the University of Illinois Frederick Seitz Materials Research Laboratory under US Department of Energy Contract No. DE-AC02-76ER01198. Work at FSU was also supported by US National Science Foundation Grant No. DMR-9315969.

# References

- [1] A. Zangwill, *Physics at Surfaces*, Ch. 11. Cambridge Univ. Press, Cambridge (1988), and references cited therein.
- [2] P. A. Rikvold, J. B. Collins, G. D. Hansen, J. D. Gunton, and E. T. Gawlinski, Mat. Res. Soc. Symp. Proc. 111, 249 (1988).
- [3] P. A. Rikvold, J. B. Collins, G. D. Hansen, and J. D. Gunton, Surf. Sci. 203, 500 (1988).
- [4] J. B. Collins, P. Sacramento, P. A. Rikvold, and J. D. Gunton, Surf. Sci. 221, 277 (1989).
- [5] L. Blum, Adv. Chem. Phys. **78**, 171 (1990).
- [6] D. A. Huckaby and L. Blum, J. Chem. Phys. **92**, 2646 (1990).

- [7] L. Blum and D. A. Huckaby, J. Chem. Phys. **94**, 6887 (1991).
- [8] D. A. Huckaby and L. Blum, J. Electroanal. Chem. **315**, 255 (1991).
- [9] D. A. Huckaby and L. Blum, Electrochem. Soc. Conf. Proc. Ser. 92-1, 139 (1992).
- [10] D. Armand and M. L. Rosinberg, J. Electroanal. Chem. **302**, 191 (1991).
- [11] P. A. Rikvold and M. R. Deakin, Surf. Sci. **294**, 180 (1991).
- [12] P. A. Rikvold, Electrochim. Acta **36**, 1689 (1991).
- [13] P. A. Rikvold and A. Wieckowski, Phys. Scr. **T44**, 71 (1992).
- [14] P. A. Rikvold, A. Wieckowski, and Q. Wang, Electrochem. Soc. Conf. Proc. Ser. 93-5, 198 (1993).
- [15] P. A. Rikvold, A. Wieckowski, Q. Wang, C. K. Rhee, and M. Gamboa, in Computer Simulation Studies in Condensed Matter Physics VI (Edited by D. P. Landau, K. K. Mon, and H. B. Schüttler), p. 162. Springer, Berlin (1993).
- [16] M. Gamboa-Aldeco, P. Mrozek, C. K. Rhee, A. Wieckowski, P. A. Rikvold, and Q. Wang, Surf. Sci. Lett. 297, L135 (1993).
- [17] L. Hightower, Q. Wang, P. A. Rikvold, M. Gamboa-Aldeco, and A. Wieckowski, *Urea Adsorption on Platinum (100) Electrodes: A Monte Carlo Simulation*. FSU-SCRI Video (1994). Electronically available in MPEG format via World Wide Web at http://www.scri.fsu.edu/~rikvold/.
- [18] P. A. Rikvold, M. Gamboa-Aldeco, J. Zhang, M. Han, Q. Wang, H. L. Richards, and A. Wieckowski, Surf. Sci., in press.
- [19] J. Zhang, P. A. Rikvold, Y.-S. Sung, and A. Wieckowski, in *Computer Simulation Studies in Condensed Matter Physics VIII* (Edited by D. P. Landau, K. K. Mon, and B. Schüttler). Springer, Berlin, in press.
- [20] J. Zhang, Y.-S. Sung, P. A. Rikvold, and A. Wieckowski, in preparation.

- [21] See, e.g., K. Binder, in Monte Carlo Methods in Statistical Physics, Second Ed. (Edited by K. Binder). Springer, Berlin (1986).
- [22] K. Binder, Ann. Rev. Phys. Chem. 43, (1992).
- [23] K. Binder and D. W. Heermann, Monte Carlo Simulation in Statistical Physics. An Introduction. Second Ed. Springer, Berlin (1992).
- [24] C. Domb, Adv. Phys. 9, 149 (1960).
- [25] K. Huang, Statistical Mechanics. Second Ed. Wiley, New York (1987).
- [26] H. E. Stanley, Introduction to Phase Transitions and Critical Phenomena. Oxford Univ. Press, Oxford (1971).
- [27] M. P. Nightingale, in *Finite-Size Scaling and Numerical Simulation of Statistical Systems* (Edited by V. Privman). World Scientific, Singapore (1990).
- [28] V. Privman, in Finite-Size Scaling and Numerical Simulation of Statistical Systems (Edited by V. Privman). World Scientific, Singapore (1990).
- [29] F. Hommeril and B. Mutaftschiev, Phys. Rev. B 40, 296 (1989).
- [30] M. Kruk, A. Patrykiejew, and S. Sokolowski, Surf. Sci., in press.
- [31] M. Gamboa-Aldeco, C. K. Rhee, A. Nahlé, Q. Wang, J. Zhang, H. L. Richards, P. A. Rikvold, and A. Wieckowski, Electrochem. Soc. Conf. Proc. Ser. 94-21, 184 (1994).
- [32] L. Blum and D. A. Huckaby, Electrochem. Soc. Conf. Proc. Ser. **93-5**, 232 (1993).
- [33] L. Blum and D. A. Huckaby, J. Electroanal. Chem. **375**, 69 (1994).
- [34] L. Blum, M. Legault, and P. Turq, J. Electroanal. Chem. **379**, 35 (1994).
- [35] M. Legault, L. Blum, and D. A. Huckaby, in *Proceedings of "Zweite Ulmer Tagung der Elektrochemischen Gesellschaft"* (Edited by D. Kolb and W. Schmickler). (1995).

- [36] See, e.g., T. L. Einstein, Langmuir 7, 2520 (1991).
- [37] A. J. Bard and L. R. Faulkner, *Electrochemical Methods: Fundamentals and Applications*. Wiley, New York (1980).
- [38] T. L. Einstein and J. R. Schrieffer, Phys. Rev. B 7, 3629 (1973).
- [39] K. H. Lau and W. Kohn, Surf. Sci. **75**, 69 (1978).
- [40] T. L. Einstein, Surf. Sci. **75**, 161L (1978).
- [41] J.-P. Muscat, Phys. Rev. B **33**, 8136 (1986).
- [42] P. J. Feibelman, Ann. Rev. Phys. Chem. 40, 261 (1989).
- [43] J. N. Glosli and M. R. Philpott, Electrochem. Soc. Conf. Proc. Ser. 93-5, 80 (1993); 93-5, 90 (1993).
- [44] A comparison of results of perturbative and nonperturbative calculations for one and the same two-dimensional lattice-gas model is given by P. A. Rikvold and M. A. Novotny, in *Condensed Matter Theories* (Edited by L. Blum and F. B. Malik), Vol. 8, p. 627. Plenum, New York (1993).
- [45] C. C. A. Günther, P. A. Rikvold, and M. A. Novotny, Phys. Rev. B 42, 10738 (1990).
- [46] D. K. Hilton, B. M. Gorman, P. A. Rikvold, and M. A. Novotny, Phys. Rev. B 46, 381 (1992).
- [47] E. Domany, M. Schick, J. S. Walker, and R. B. Griffiths, Phys. Rev. B 18, 2209 (1978).
- [48] E. Domany and M. Schick, Phys. Rev. B **20**, 3828 (1979).
- [49] M. Schick, Prog. Surf. Sci. 11, 245 (1981).
- [50] P. A. Rikvold, K. Kaski, J. D. Gunton, and M. C. Yalabik, Phys. Rev. B 29, 6285 (1984).
- [51] T. Aukrust, M. A. Novotny, P. A. Rikvold, and D. P. Landau, Phys. Rev. B 41, 8772 (1990).

- [52] E. Protopopoff and P. Marcus, Surf. Sci. **169**, L237 (1986).
- [53] J. O. Bockris, M. Green, and D. A. J. Swinkels, J. Electrochem. Soc. 111, 743 (1964).
- [54] J. O. Bockris and D. A. J. Swinkels, J. Electrochem. Soc. 111, 736 (1964).
- [55] B. D. Damaskin, O. A. Petrii, and V. V. Batrakov, *Adsorption of Organic Compounds on Electrodes*, pp. 256-257. Plenum, New York (1971).
- [56] J. Zhang, P. A. Rikvold, and A. Wieckowski, in preparation.
- [57] M. Rubel, C. K. Rhee, A. Wieckowski, and P. A. Rikvold, J. Electroanal. Chem. 315, 301 (1991).
- [58] D. M. Kolb, Z. Phys. Chem. Neue Folge **154**, 179 (1987).
- [59] M. Zei, G. Qiao, G. Lempfuhl, and D. M. Kolb, Ber. Bunsen Ges. Phys. Chem. 91, 3494 (1987).
- [60] J. W. Schultze and D. Dickertmann, Surf. Sci. 54, 489 (1976).
- [61] A. Itai, H. Yamada, T. Okamoto, and Y. Iitaka, Acta Cryst. B33, 1816 (1977).
- [62] See, e.g., Table 1.4 of C. Kittel, Introduction to Solid State Physics, Sixth Ed. Wiley, New York (1986).
- [63] A. Peremans and A. Tadjeddine, Phys. Rev. Lett. 73, 3010 (1994).
- [64] A. Tadjeddine and A. Peremans, Surf. Sci., in press.
- $[65]\,$  Z. Shi and J. Lipowski, J. Electroanal. Chem.  ${\bf 364},\,289$  (1994).
- [66] Z. Shi and J. Lipowski, J. Electroanal. Chem. **365**, 303 (1994).
- [67] Z. Shi, S. Wu, and J. Lipowski, Electrochim. Acta 40, 9 (1995).
- [68] C. Pascard-Billy, Acta Cryst. 18, 829 (1965).
- [69] D. P. Landau, Phys. Rev. B 27, 5604 (1983).

- [70] R. J. Baxter, Exactly Solved Models in Statistical Mechanics, Ch. 11.8. Academic, London (1982).
- [71] O. M. Magnussen, J. Hotlos, R. J. Nichols, D. M. Kolb, and R. J. Behm, Phys. Rev. Lett. 64, 2929 (1990).
- [72] G. J. Edens, X. Gao, and M. J. Weaver, J. Electroanal. Chem. 375, 357 (1994).

#### **Figure Captions**

Figure 1: The lattice-gas model used in Refs. [14, 15, 16, 17, 18] to describe the coadsorption of urea (U) and hydrogen (H) on Pt(100). The relative positions of hydrogen ( $\bullet$ ) and urea (filled rectangles) correspond to the effective interactions in Eq. (1), which are invariant under symmetry operations on the lattice. The values used in Refs. [16, 17, 18] were (in kJ/mol)  $\Phi_{\rm HH}^{(1)} = -2.0$ ,  $\Phi_{\rm HU}^{(1)} = -8.0$ ,  $\Phi_{\rm HU}^{(2)} = -4.0$ ,  $\Phi_{\rm UU}^{(1)} = -13.0$ ,  $\Phi_{\rm UU}^{(2)} = -10.0$ ,  $\Phi_{\rm UU}^{(3)} = -5.9$ ,  $\Phi_{\rm UU}^{(4)} = -0.5$ ,  $\Phi_{\rm UU}^{(5)} = -2.5$ ,  $\Phi_{\rm UU}^{(6)} = -3.0$ ,  $\Phi_{\rm UU}^{(7)} = +0.25$ ,  $\Phi_{\rm UU}^{(8)} = -2.0$ , and the effective electrovalences were taken as  $z_{\rm H} = +1$  and  $z_{\rm U} = -1$ . After Ref. [18].

Figure 2: The lattice-gas model used in Refs. [19, 20] to describe the UPD of copper (C) on Au(111) in the presence of sulfate (S). The relative positions of copper ( $\bullet$ ) and sulfate ( $\triangle$ ) correspond to the effective interactions in Eq. (1), which are invariant under symmetry operations on the lattice. The numbers are the corresponding values of  $\Phi_{XY}^{(l)}$  used in Refs. [19, 20], given in kJ/mol. After Ref. [20].

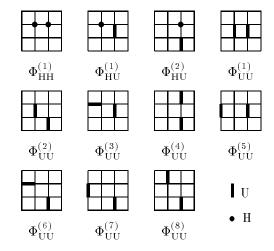
Figure 3: Ground-state diagram for the lattice-gas model of urea on Pt(100), shown in the  $(\bar{\mu}_{\rm U}, \bar{\mu}_{\rm H})$  plane. The model parameters are the same as in Fig. 1. (a) The zero-temperature phase boundary between the  $c(2\times4)$  phase with  $\Theta_{\rm U}=1/4$ , indicated as c(2×4)U in the figure, and the (1×1) phase with  $\Theta_{\rm H}=1$ , indicated as  $(1\times1)H$ , is shown as a solid line together with the electrochemical potentials corresponding to room-temperature experimental (× connected by dotted lines) and simulated (+ connected by dashed lines) CV peak positions. The solid arrows represent positive-going E scans from  $-106 \,\mathrm{mV}$  to  $-56 \,\mathrm{mV}$ versus Ag/AgCl at room temperature. From left to right they represent [U]=2.0, 1.0, and 0.5 mM. Simulated and experimental CV currents along the scan at 1.0 mM are shown in Fig. 6. (b) A full ground-state diagram for the interactions used, showing all the phases present. The phase indicated in the figure by c(2×4)UU has  $\Theta_U=1/2$ , (1×3)U has  $\Theta_U=1/3$ , ( $\sqrt{2}\times\sqrt{2}$ )H has  $\Theta_{\rm H}=1/2$ , and  $(1\times1)0$  is the empty lattice. The phase regions outside the dotted box, which corresponds to panel (a), are not believed to be experimentally relevant. After Ref. [18].

Figure 4: Ground-state diagram for the lattice-gas model of copper UPD on Au(111) in sulfuric-acid electrolyte, shown in the  $(\bar{\mu}_{\rm S}, \bar{\mu}_{\rm C})$  plane. The model parameters are the same as in Fig. 2. The solid lines represent zero-temperature phase boundaries, and the dotted lines represent voltammetric scan paths at room temperature. The scan path labeled "1" is fitted to an experiment with an electrolyte containing 1.0 mM CuSO<sub>4</sub> [20], whereas "2" and "3" represent simulations corresponding to 5.0 mM and 0.2 mM sulfate with 1.0 mM Cu<sup>2+</sup>, respectively. The end points of the dotted lines, marked +, correspond to electrode potentials 55 mV (upper left) and 245 mV (lower right) versus Cu/Cu<sup>+</sup>, respectively. The phases are indicated as  $(X \times Y)_{\theta_{\rm C}}^{\theta_{\rm S}}$ . The solid squares indicate the left-hand peak positions, and the solid diamonds indicate the right-hand peak positions of simulated room-temperature CV currents, such as that shown in Fig. 7. After Ref. [20].

Figure 5: Electrosorption of naphthalene on copper in alkaline aqueous environment. Experimental (data points connected by dotted straight lines) [53] and fitted numerical adsorption isotherms (solid curves) [11] are shown. The lattice-gas parameters, determined by a nonlinear least-squares fit, are also given. From below to above, the isotherms correspond to naphthalene concentrations of 2.5, 5.0, 7.5, and  $10.0 \times 10^{-5}$  M. After Refs. [11, 12, 13].

Figure 6: Cyclic voltammogram (CV) for urea adsorbed on Pt(100) in  $0.1\,\mathrm{M}$   $HClO_4$  at room temperature. Experimental (dashed curves) and simulated ( $\diamondsuit$  and solid curve) normalized CV currents,  $i/(\mathrm{d}E/\mathrm{d}t)$  in elementary charges per mV per Pt(100) unit cell, at  $1.0\,\mathrm{mM}$  bulk urea. The two dashed curves are representative negative-going voltammograms, and their differences indicate the experimental uncertainty. The model parameters are given in the caption of Fig. 1. After Ref. [18].

Figure 7: Cyclic voltammogram (CV) for copper UPD on Au(111) at room temperature, corresponding to the scan path labeled "1" in Fig. 4. Experimental (dashed curve) and preliminary simulated (solid curve), normalized CV currents [20]. Left scale: CV current density. Right scale: normalized CV current density, i/(dE/dt), in electrons per mV per Au(111) unit cell. The model parameters are given in Fig. 2. After Ref. [20].



$$\Phi_{\text{CC}}^{(1)}$$
 $\Phi_{\text{CC}}^{(2)}$ 
 $\Phi_{\text{SC}}^{(1)}$ 
 $\Phi_{\text{SC}}^{(1)}$ 
 $\Phi_{\text{SC}}^{(1)}$ 
 $\Phi_{\text{SC}}^{(1)}$ 
 $\Phi_{\text{CC}}^{(1)}$ 
 $\Phi_{\text{SC}}^{(1)}$ 
 $\Phi_{\text{CC}}^{(1)}$ 
 $\Phi_{\text{CC}}^$ 

